Electronic Supplementary Information for:

Ultrafast Action Chemistry in Slow Motion: Atomistic Description of the Excitation and Fluorescence Processes in an Archetypal Fluorescent Protein

Pau Armengol,[a] Lasse Spörkel,[b] Ricard Gelabert[a,*], Miquel Moreno,[a] Walter Thiel[b,*] and José M. Lluch[a,c]

[a] *Departament de Química, Universitat Autònoma de Barcelona, 08193 Bellaterra, Barcelona, Spain,* [b] *Max-Planck-Institut für Kohlenforschung, Kaiser-Wilhelm-Platz 1, 45470 Mülheim an der Ruhr, Germany, and* [c] *Institut de Biotecnologia i de Biomedicina, Universitat Autònoma de Barcelona, 08193 Bellaterra, Barcelona, Spain*

Contents

1 Time Evolution of Selected Geometrical Parameters

The main article describes the time evolution of several parameters to show how the structure of the fluorescent protein accommodates to the photoexcitation. Here we address the time evolution of the entire swarm of more than 300 individual QM/MM MD simulations (more precisely, of those that are still in the photoexcited state at a given instant). Fig. S1 to S3 show 2-dimensional histograms that indicate how many of these individual trajectories of the swarm have a specific value of each geometric parameter at a given time, and they also provide the root-mean-square (RMS) value of the distribution at each time frame.

The distances between donor and acceptor, as well as the position of the transferred proton, follow the general behavior described in the main text. The spread of the distributions increases in a natural way with increasing time (Fig. S1). As stated in the main text, the average distance between the phenolic oxygen and the oxygen of Tyr145 decreases during the dynamics after photoexcitation. In the ground state this distance obeys a bimodal distribution with two maxima, one around 3.0 Å and another less pronounced one around 4.5Å.[1] Panel (c) in Fig. S1 shows that this decrease is actually due to the depletion of the outer maximum since most of the population shifts to fill the inner maximum: Tyr145 does not only move on average closer to the chromophore, but it actually vacates the configuration in which it was farthest away.

We have also checked the distribution of the dihedrals that define the planarity of the two rings of the chromophore (or the lack thereof). The average value of the dihedral τ (defined in the main text) changes upon photoexcitation by about 40°away from planarity. Analysis of the distribution (Panel (a) in Fig. S2) shows the existence of two populations, one close to planarity (the larger one) and another at ∼240°, with an almost perpendicular conformation of the imidazolinone ring, which is populated after 0.1 ps. For the other angular parameters in Fig. S2 normal distributions are observed throughout.

Finally, Fig. S3 shows the distribution of the two angles that have been used to indicate the proximity to the two conical intersections, T-like or P-like. In both cases the color histogram shows that the corresponding dihedral develops two different populations (becomes bimodal) for times of 0.1 ps and beyond. The distribution of the dihedral characterizing a T-type CI (θ, panel (a) in Fig. S3) shows that most systems are found around $\theta \sim 180°$, but a certain population appears around 270° at times over 0.1 ps. This is the part of the swarm of trajectories that is moving close to the T CI and decays to the ground state as time increases. For the P-type CI, panel (b) in Fig. S3 shows a small population that peaks at $\rho \sim 120°$ after 0.1 ps and later.

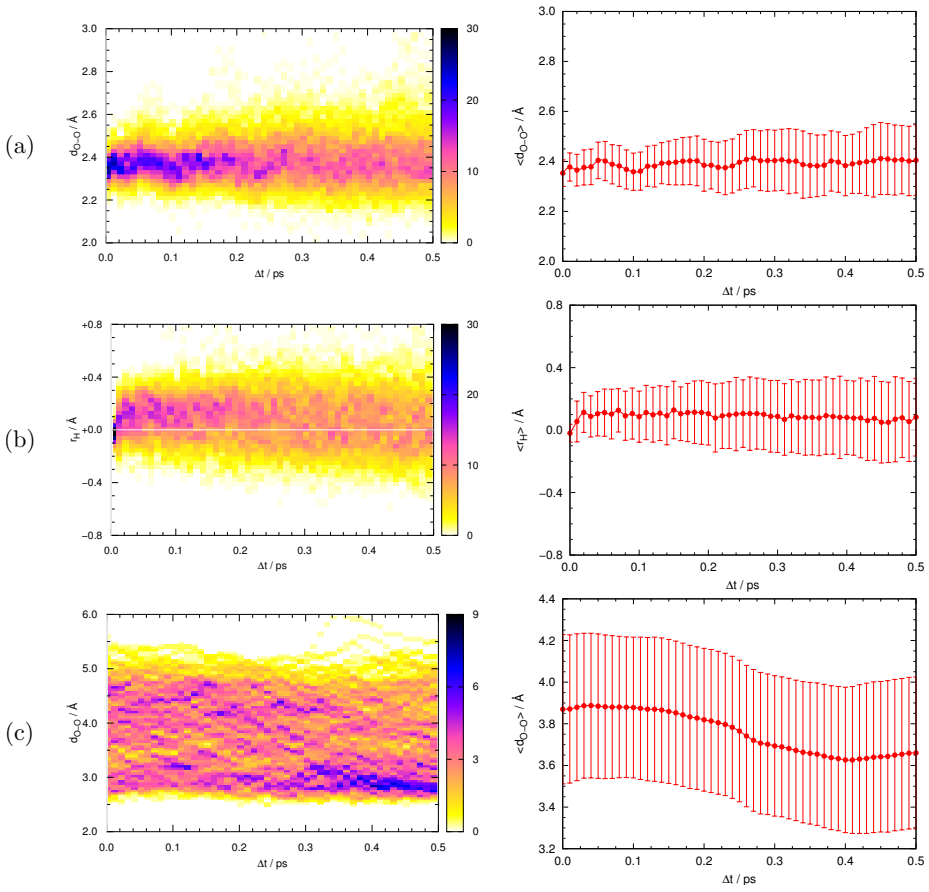

Figure S1: Time evolution of (a) the donor-acceptor distance, (b) the proton position according to Eq 5, and (c) the distance between the oxygens of Tyr66 (in the chromophore) and Tyr145, for the full swarm of trajectories. Left column: 2-dimensional histogram depicting with darker colors the regions with higher structure count; right column: time evolution of the average values of the distances. The vertical bars represent one standard deviation in each case.

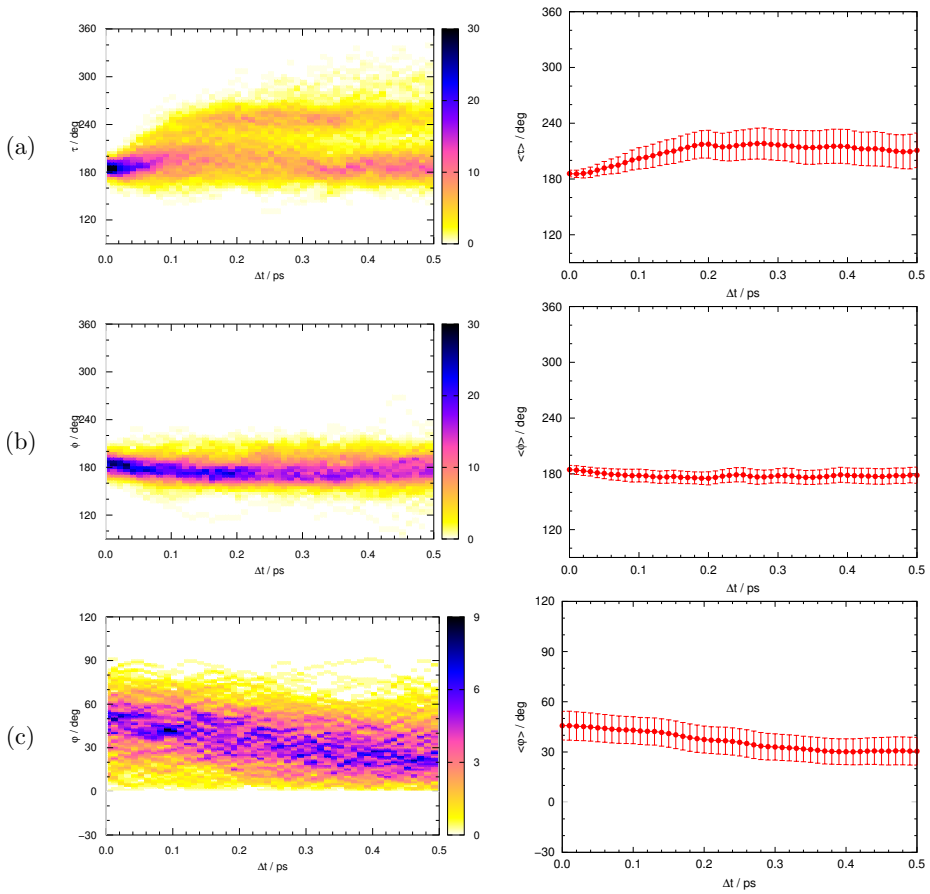

Figure S2: Time evolution of the planarity of the chromophore-Asp148 unit in terms of (a) the τ dihedral, (b) the ϕ dihedral and (c) the φ dihedral, for the full swarm of trajectories (see the main text for a definition of these angles). Left column: 2-dimensional histogram depicting with darker colors the regions with higher structure count; right column: time evolution of the average values of the distances. The vertical bars represent one standard deviation in each case.

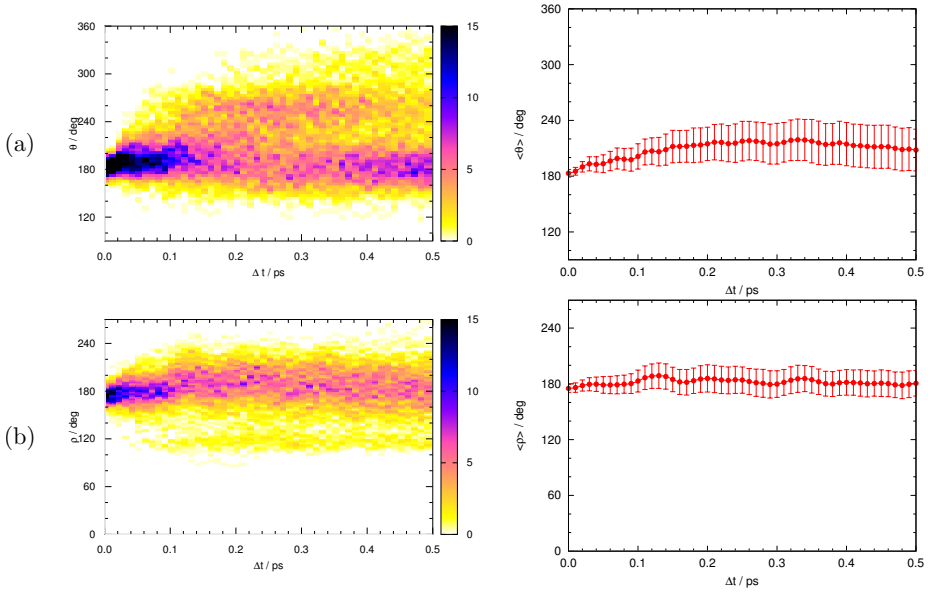

Figure S3: Time evolution of the dihedral angles that identify the proximity of non-radiative relaxation channels: (a) θ and (b) ρ, for the full swarm of trajectories. See main text for a definition of these angles. Left column: 2-dimensional histogram depicting with darker colors the regions with higher structure count; right column: time evolution of the average values of the distances. The vertical bars represent one standard deviation in each case.

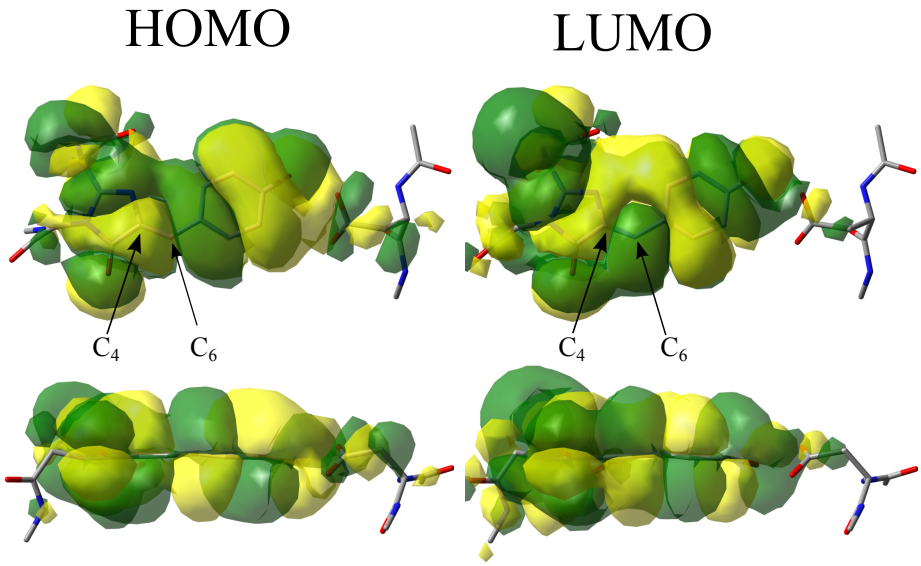

Figure S4: Molecular orbitals that are involved in the photoexcitation: on the left the HOMO orbital (from which the excited electron is taken) and on the right the LUMO orbital (where the excited electron ends up). The top row shows both orbitals as seen from above the chromophore plane, and the bottom row displays the orbitals as seen from the molecular plane. There is a nodal plane in the LUMO between atoms C_4 and C_6.

2 Molecular Orbitals Involved in the Photoexcitation

Fig. S4 shows a picture of the (local) π molecular orbitals that are involved in the photoexcitation. The determinant with the largest weight in the CI expansion corresponds to the π-HOMO $\rightarrow$ π-LUMO single excitation. These orbitals are analogous to those already published for the same system.[2] Among the changes unleashed by the photoexcitation, we note here the creation of a nodal surface across the bond between C_4 and C_6 in the LUMO (which is absent in the HOMO). This helps to understand why during the dynamics many systems undergo a torsion around this bond, which loses its double bond character upon photoexcitation.

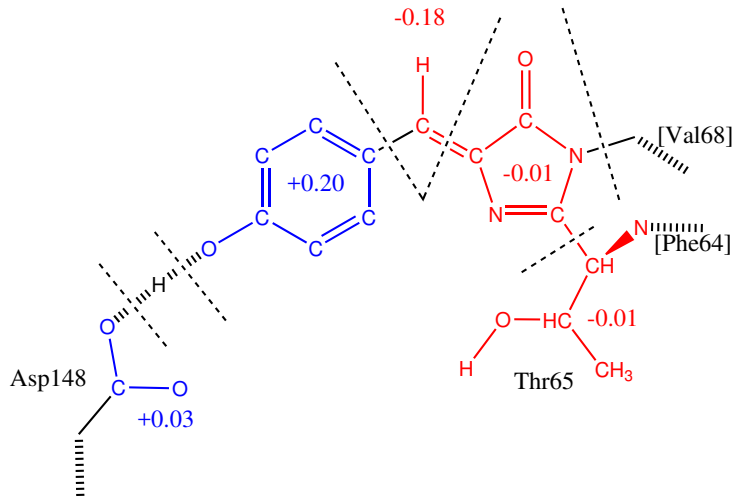

Figure S5: Changes in fragment charges due to photoexcitation. Red (blue) figures indicate a net increase (decrease) of negative charge.

3 Charge Redistribution Caused by Photoexcitation

A natural bond orbital (NBO) analysis has been carried out on a single snapshot of the QM/MM MD simulation to assess the changes caused in the electronic distribution upon photoexcitation. Fig. S5 shows the corresponding overall variation of charges, computed as the difference between the NBO charges of each fragment in the photoactive and the ground electronic state. Table S1 lists the values of the NBO charges in the ground and the photoactive state for each moiety.

The net effect of the photoexcitation, in terms of gross charge redistribution, is a displacement of about 0.2 electrons from the phenolic moiety, mainly to the methine bridge.

4 Time Evolution of the Average Emission Energy

Fig. S6 shows the time evolution of the excitation energy *vs.* the classical proton position. It is possible to discern at a glance the displacement of the cloud of points from top left to bottom right, implying that along the average motion of the proton from donor to acceptor, the computed excitation energies shift to lower values.

Moiety	$Q(S_0)$ / a.u.	$Q(S_1)$ / a.u.	ΔQ / a.u.
Phenolic	–0.59	–0.39	+0.20
Methine bridge	+0.17	–0.0057	–0.18
Imidazolinone	–0.60	–0.61	–0.0092
Thr65	–0.30	–0.31	–0.017
Asp148 (Carboxylate)	–0.68	–0.67	+0.0033
H	+0.52	+0.52	–0.0020

Table S1: NBO charges of different fragments of the chromophore-Asp148 unit in the ground electronic state and the photoactive excited electronic state, and net change of these charges upon photoexcitation (see also Fig. S5). The charges have been computed for the atoms shown, including the corresponding hydrogens where applicable. The given net charges in S_0 and S_1 do not add up to –1 because the side chains of the residues Phe64, Val68 and Asp148 have not been considered in this analysis.

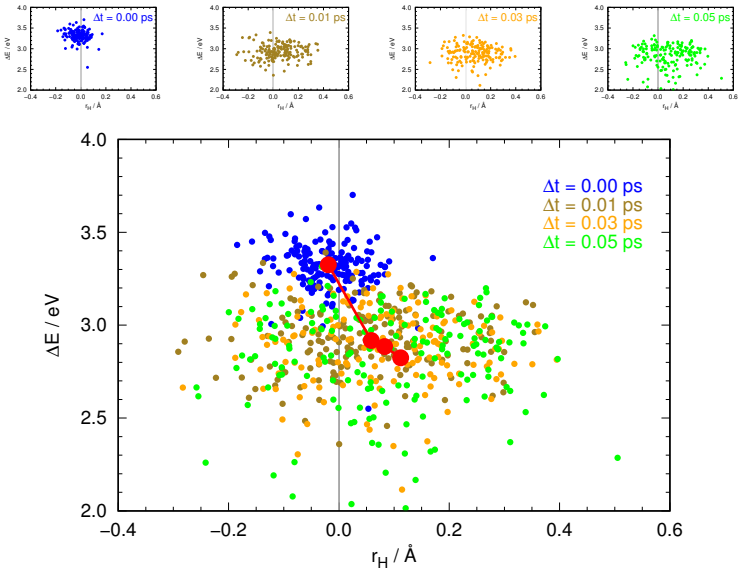

Figure S6: Relationship between the position of the proton on the proton transfer reaction coordinate (Eq 5) and the emission energy in the early stages (up to 50 fs). The upper panels depicts this relationship for specific snapshots at Δt= 0, 10, 30 and 50 fs, respectively. The bottom panel presents all data together, plus the path followed by the average excitation energy as a function of the average proton position (red dots and path). The red dot for $\Delta t = 0$ is at the top-left, and that for $\Delta t = 50$ fs is at the bottom-right.

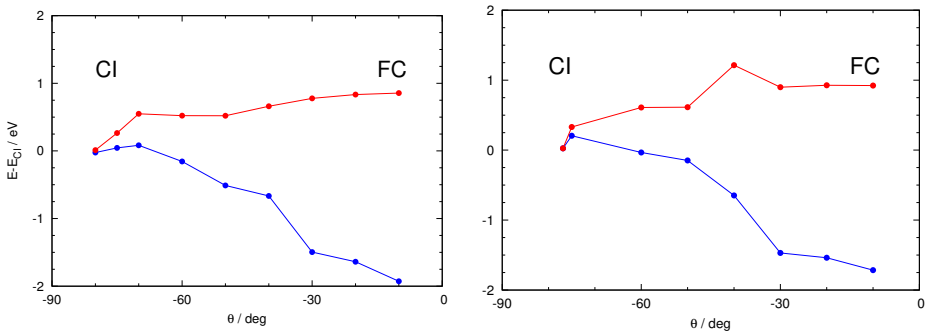

Figure S7: S_1-relaxed potential energy profile leading from the Franck-Condon region (FC) to the T-type CI region (CI) computed at the QM/MM level; red: optimized S_1 energies; blue: single-point S_0 energies. Left panel: QM = OM2/MRCI; right panel: QM = TDDFT.

5 Barriers on the Way from FC region to T- and P-type CIs

The ultrafast non-radiative decay indicates an exaggerated accessibility of the CI region at the QM(OM2/MRCI)/MM level. To check this further, we computed a relaxed potential energy profile in the S_1 state to generate a minimum-energy path from the Franck-Condon region to the T-type CI region taking the dihedral θ as the reaction coordinate (running the computations in forward and backward direction until convergence to overcome hysteresis problems). The left panel of Fig. S7 shows the resulting stable potential energy profile obtained at the QM(OM2/MRCI)/MM level (same as in the MD simulations): the potential energy profile is downhill and barrierless. For comparison, the right panel of the same Figure presents an S_1-relaxed potential energy profile computed at the QM(TDDFT)/MM level in a single pass (without going back and forth): it has a small barrier, consistent with previous *ab initio* QM/MM results;[3] we have also computed a second such QM(TDDFT)/MM profile which reaches the CI region on an uphill path in the S_1 state (data not shown). Apparently the QM(OM2/MRCI)/MM method, with the choice of active space used presently, affords an excited-state surface on which the approach to the CI region is too facile, compared with higher-level electronic structure methods. Hence, the QM(OM2/MRCI)/MM simulations will overestimate the rate of decay through the T-type conical intersection.

The corresponding path to the P-type CI has been explored at OM2/MRCI level taking the dihedral ρ as the reaction coordinate. A relaxed potential energy profile is shown in Fig. S8. In this case, the potential energy profile has a small potential energy barrier in the S_1 state. This agrees with the observation that the decay through the P-type CI occurs much less frequently in our simulations than the decay through the T-type CI.

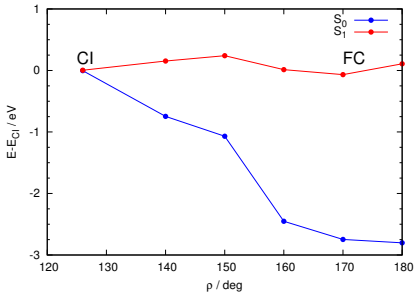

Figure S8: S_1-relaxed potential energy profile leading from the Franck-Condon region (FC) to the P-type CI region (CI) computed at the QM(OM2/MRCI)/MM level. Abscissa values: dihedral angle ρ.

The reason why OM2/MRCI might perform worse in describing the region surrounding the CIs is unknown. Nevertheless, one possibility is the choice of MOs used in the description of the active space. This choice, set forth in the main text, was conceived to provide a good description of the π system during the main chemical event (the proton transfer). However, the approach of the CI regions involves areas of configurational space with a strongly twisted chromophore moiety, and thus it is possible that the corresponding out-of-plane torsions require of a different choice of MOs to be described appropriately. Of course, to describe at the same time proton transfer and CI transit with a single active space, the latter should consist of the union of the sets of MOs adequate for each process, which is probably too large to be practical.

6 P-type CI in the Isolated Chromophore

Fig. S9 shows unrelaxed potential energy profiles determined for the isolated chromophore at the DFT/TDDFT level (methodology as described in the main text). ρ is the angle $C_4C_2O_3N_1$. Structures were generated by keeping both rings of the chromophore coplanar at the ground-state equilibrium positions while moving the oxygen atom of the imidazolinone moiety out of plane. DFT/TDDFT was used to compute the ground state/excitation energy, using the CAM-B3LYP functional and the 6-31G(d,p) basis set.

References

[1] P. Armengol, R. Gelabert, M. Moreno and J. M. Lluch,*J. Phys. Chem. B*, 2015, **119**, 2274 – 2291.

[2] P. Armengol, R. Gelabert, M. Moreno and J. M. Lluch, *Org. Biomol. Chem.*, 2014, **12**, 9845 – 9852.

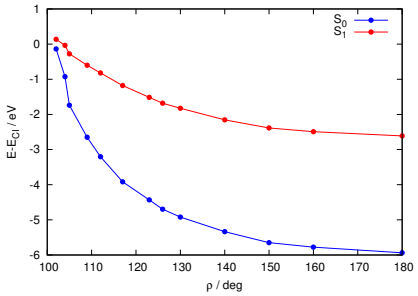

Figure S9: Energy (relative to the P-type CI) of structures of the gas-phase chromophore as a function of angle ρ. Structures with all atoms of the chromophore rings in a plane, except for the oxygen in the imidazolinone moiety (see text).

[3] Q. Zhang, X. Chen, G. Cui, W. Fang and W. Thiel, *Angew. Chem. Int. Ed.*, 2014, **53**, 8649 – 8653.